MINERVA: A facile strategy for SARS-CoV-2 whole genome deep sequencing of clinical samples

Chen Chen[a,#], Jizhou Li[b,#], Lin Di[c,d,#], Qiuyu Jing[e,#], Pengcheng Du[a,#], Chuan Song[a], Jiarui Li[a], Qiong Li[b], Yunlong Cao[c], X. Sunney Xie[c], Angela R. Wu[e,f,*], Hui Zeng[a,*], Yanyi Huang[c,g,h,i,*], Jianbin Wang[b,i,j,*]

[a] Institute of Infectious Diseases, Beijing Ditan Hospital, Capital Medical University and Beijing Key Laboratory of Emerging Infectious Diseases, Beijing 100015, China.

[b] School of Life Sciences, Tsinghua-Peking Center for Life Sciences, Tsinghua University, Beijing 100084, China.

[c] Beijing Advanced Innovation Center for Genomics (ICG), Biomedical Pioneering Innovation Center (BIOPIC), Peking-Tsinghua Center for Life Sciences, Peking University, Beijing 100871, China.

[d] School of Life Sciences, Peking University, Beijing 100871, China.

[e] Division of Life Science, Hong Kong University of Science and Technology, Hong Kong SAR, China.

[f] Department of Chemical and Biological Engineering, Hong Kong University of Science and Technology, Hong Kong SAR, China

[g] College of Chemistry and Molecular Engineering, Beijing 100871, China

[h] Institute for Cell Analysis, Shenzhen Bay Laboratory, Guangdong 518132, China

[i] Chinese Institute for Brain Research (CIBR), Beijing 102206, China.

[j] Beijing Advanced Innovation Center for Structural Biology (ICSB), Tsinghua University, Beijing 100084, China.

[#] These authors contributed equally to this work.

* Corresponding authors: jianbinwang@tsinghua.edu.cn (J.W.), yanyi@pku.edu.cn (Y.H.), zenghui@ccmu.edu.cn (H.Z.) and angelawu@ust.hk (A.R.W.).

Abstract

The novel coronavirus disease 2019 (COVID-19) pandemic poses a serious public health risk. Analyzing the genome of severe acute respiratory syndrome coronavirus 2 (SARS-CoV-2) from clinical samples is crucial for the understanding of viral spread and viral evolution, as well as for vaccine development. Existing sample preparation methods for viral genome sequencing are demanding on user technique and time, and thus not ideal for time-sensitive clinical samples; these methods are also not optimized for high performance on viral genomes. We have developed MetagenomIc RNA EnRichment VirAl sequencing (MINERVA), a facile, practical, and robust approach for metagenomic and deep viral sequencing from clinical samples. This approach uses direct tagmentation of RNA/DNA hybrids using Tn5 transposase to greatly simplify the sequencing library construction process, while subsequent targeted enrichment can generate viral genomes with high sensitivity, coverage, and depth. We demonstrate the utility of MINERVA on pharyngeal, sputum and stool samples collected from COVID-19 patients, successfully obtaining both whole metatranscriptomes and complete high-depth high-coverage SARS-CoV-2 genomes from these clinical samples, with high yield and robustness. MINERVA is compatible with clinical nucleic extracts containing carrier RNA. With a shortened hands-on time from sample to virus-enriched sequencing-ready library, this rapid, versatile, and clinic-friendly approach will facilitate monitoring of viral genetic variations during outbreaks, both current and future.

Introduction

As of May 22, 2020, the ongoing COVID-19 viral pandemic has affected 5 million people in over 200 countries and territories around the world, and has claimed more than 320 thousand lives[1]. Closely monitoring the genetic diversity and distribution of viral strains at the population level is essential for epidemiological tracking, and for understanding viral evolution and transmission; additionally examining the viral heterogeneity within a single individual is imperative for diagnosis and treatment[2]. The disease-causing pathogen, severe acute respiratory syndrome coronavirus 2 (SARS-CoV-2), was identified from early disease cases and its draft genome sequenced within weeks, thanks to the rapid responses from researchers around the world[3-6]. The initial SARS-CoV-2 draft genome was obtained independently from the same early COVID-19 patient samples using various conventional RNA-seq sequencing library construction methods. Although these library construction methods successfully generated a draft genome, several drawbacks hinder the use of these methods for routine viral genome sequencing from the surge of clinical samples during an outbreak.

One direct library construction approach which was used to generate the SARS-CoV-2 draft genome[3-6] essentially captures each sample's entire metatranscriptome, in which SARS-CoV-2 is just one species among many. The abundance of SARS-CoV-2 in clinical swabs, sputum, and stool samples is often low[2,7], therefore this catch-all method requires deeper sequencing of each sample in order to obtain sufficient coverage and depth of the whole viral genome, which increases the time and cost of sequencing. Target enrichment with spiked-in primers can improve SARS-CoV-2 genome coverage[8], but the reliance on specific primers inherently limits this approach for the profiling of fast evolving viruses such as coronaviruses. The same limitation applies to multiplex RT-PCR-based strategies[9]. Additionally, once the sample is subject to targeted amplification during the initial reverse transcription (RT) steps, its metatranscriptomic information is lost forever.

Currently, the most comprehensive strategy is the combination of metatranscriptomics profiling with post-library SARS-CoV-2 target enrichment[9]. However, in most conventional RNA-seq methods, the double-strand DNA ligation (dsDL) portion of the protocol is

usually the most demanding on hands-on time and user technique[10]. When superimposed on the target enrichment process, these labor-intensive and lengthy protocols become impractical for routine use in the clinic, much less for the timely monitoring of viral genetics and evolution on large volumes of samples during an outbreak. Furthermore, due to the low molecular efficiency of dsDL, these protocols also require a high amount of input material, further restricting their application on clinical samples.

Summarily, although next generation sequencing platforms are high-throughput and have short turn-around time, library construction from samples – whether including targeted enrichment or not – remains a major bottleneck. To broadly apply viral sequencing on clinical samples, especially during outbreaks when biomedical resources are already limited, a rapid, simple, versatile, and scalable sample library construction method that does not compromise on performance is urgently needed.

Recently, we reported a new RNA-seq library construction strategy that aims to address some of these challenges: SHERRY avoids the problematic dsDL step in library construction by taking advantage of the newly discovered Tn5 tagmentation activity on RNA/DNA hybrids, to directly tag RNA/cDNA fragments with sequencing adapters[10]. As such, SHERRY has minimal sample transfers and greatly reduced hands-on time, making it simple, robust, and suitable for inputs ranging from single cells to 200 ng total RNA. We now combine the advantages of a tailored SHERRY protocol, which improved coverage of whole metatranscriptome, with a simplified post-library target enrichment protocol. MetagenomIc RNA EnRichment VirAl sequencing or MINERVA, is an easy-to-use, versatile, scalable, and cost-effective protocol that yields high-coverage high-depth SARS-CoV-2 genome, while preserving the sample's rich metatranscriptomic profile. The hands-on time required from clinical sample to sequencing-ready library using conventional approaches without enrichment is 190 min; MINERVA requires only 100 min hands-on time, and if deep viral coverage is desired, an additional 90 min for post-library enrichment, totaling 190 min for the entire workflow (**Fig. S1**), making MINERVA practical for high-volume, routine clinical use. We applied MINERVA to various types of COVID-19 samples and successfully obtained up to 10,000-fold SARS-CoV-2 genome enrichment.

116 This strategy will facilitate all studies regarding SARS-CoV-2 genetic variations in the
117 current pandemic, and can also be applied to other pathogens of interest.
118
119 **Results**
120 **Metagenomic RNA enrichment viral sequencing (MINERVA).** To analyze both
121 metagenomics and SARS-CoV-2 genetics from COVID-19 patient samples, we
122 developed a two-stage metagenomic RNA enrichment viral sequencing strategy termed
123 MINERVA (**Fig. 1A**). First, we employed a SHERRY-based RNA-seq pipeline for
124 metagenomic analysis. Since clinical samples may contain DNA, RNA, and possibly
125 carrier RNA, MINERVA starts with ribosomal RNA (rRNA) removal and optional
126 simultaneous carrier RNA removal, followed by DNase I treatment. The remaining RNA
127 is then subject to standard SHERRY. Previously we observed 3' bias in SHERRY libraries;
128 to address this, we used 10 ng mouse 3T3 cell total RNA as starting material, and tested
129 whether adding random decamers (N10) during RT could improve coverage evenness
130 (**Fig. S2**). Compared with the standard SHERRY protocol, which uses 1 μM T30VN primer
131 during RT, the supplement of 1 μM N10 indeed improves gene body coverage evenness,
132 presumably by improving the RT efficiency. When the N10 concentration was further
133 increased to 10 μM, we observed almost no coverage bias in the gene body. The high
134 N10 concentration can result in an increased rRNA ratio in the product, sometimes as
135 high as 90%, but MINERVA employs rRNA removal as the first step prior to RT, thus
136 negating this problem. We also performed enzyme titration with homemade and
137 commercial Tn5 transposomes. Based on these N10 and Tn5 titration results, we used
138 10 μM N10 during RT and 0.5 μl V50 for each 20-μl tagmentation reaction in all following
139 experiments. The whole procedure from nucleic acid to metagenomic sequencing-ready
140 library, including wait time, takes 5.5 hours (**Fig. S1**).
141
142 For target enrichment, we first quantified SARS-CoV-2 abundance in each metagenomic
143 sequencing library using an N gene qPCR assay, and pooled eight libraries based on
144 quantification results. Then we performed standard in-solution hybridization on the pooled
145 library with biotinylated RNA probes covering the whole viral genome. The enrichment
146 procedure takes 7~13 hours; the entire MINERVA pipeline can be completed within 12~18

147 hours.

148

149 **MINERVA is compatible with COVID-19 samples.** To evaluate its performance on
150 clinical samples, we applied MINERVA on 143 samples collected from 91 COVID-19
151 patients, with samples types including pharyngeal swabs, sputum, stool, and semen.
152 These patients were admitted to Ditan Hospital within a three-month period from January
153 to April 2020, presenting different symptom severity (**Fig. 1B and Table S1-S3**). Some
154 patients were re-sampled longitudinally to investigate temporal and intra-host viral
155 heterogeneity. We first tested the effect of sample input volume on MINERVA results.
156 Using just 2.7-ul of sample input led to satisfactory SARS-CoV-2 coverage, and scaling
157 up the reaction volume to 5.4-ul further improved the MINERVA data quality (**Fig. 1C**).
158 Using the same samples and at the same sequencing depth, more input in a higher
159 reaction volume generated deeper SARS-CoV-2 genome coverage.

160

161 Carrier RNA, which is widely used in viral DNA/RNA extraction before RT-qPCR assays,
162 severely impacts high-throughput sequencing analysis. Therefore, most RT-qPCR
163 positive clinical samples are not amenable to further viral genetic studies. We explored
164 the effect of adding polyT oligos during the rRNA removal step to simultaneously remove
165 spike-in polyA RNA and carrier RNA. By incorporating this step in MINERVA, we
166 successfully avoided the overwhelming representation of unwanted RNA sequences
167 while retaining desired metagenomic and SARS-CoV-2 information (**Fig. 1D and 1E**).

168

169 **MINERVA captures metagenomic signatures of COVID-19 samples.** We
170 benchmarked MINERVA against conventional dsDL strategies in head-to-head
171 comparisons of the first 79 clinical samples sequenced. On average, we sequenced 1-3
172 Gbp for each MINERVA library, and nearly 100 Gbp for each dsDL library (**Fig. S3**). The
173 metagenomic compositions of SHERRY and dsDL libraries were comparable: total virus,
174 fungus, and bacteria ratios were highly concordant between the two methods (**Fig. S4**);
175 bacterial heterogeneity as measured by entropy is also correlated between the two.

176

177 We performed various analyses to explore the metagenomic composition of different

178 samples types, and to assess whether metagenomic signatures correlate with disease
179 severity. First and foremost, we observed that the metagenomic composition of different
180 sample types show body site-specific features. Principle components analysis of bacterial
181 sequences showed a clear separation between stool samples and the other sample types
182 along PC1 (**Fig. 2A**), and this is reflected in analysis at both the genus and species levels,
183 conveying the unique microbial environment of this body site. This phenomenon is most
184 prominently reflected by the bacterial composition, but is also somewhat reflected in the
185 viral composition (**Fig. S5**). We then identified the specific microbes that drive this
186 separation of sample types, and found some microbes to be body site-specific. For
187 example, stool samples contained *Bacteroides*, whereas the pharyngeal and sputum
188 samples were rich in *Streptococcus* (**Fig. 2B and S5**); a few samples are highly abundant
189 in known pathogenic species such as *Candida*, which is only found in orally obtained
190 samples (**Fig. S5**). There also appears to be separation between samples by COVID-19
191 symptom severity along PC2 (**Fig. 2A**), which is supported by our analysis of specific
192 microbial species (**Fig. 2B**). We found the bacterial metagenomic signature could be used
193 to cluster most of the samples from "Critical" patients: samples from severe and critical
194 condition patients are abundant in *Pseudomonas,* whereas *Streptococcus* is abundant in
195 less severe condition samples.
196
197 To further explore how bacterial composition reflects disease severity, we computed the
198 bacterial ratio, bacterial species richness, and the Shannon Diversity Index for each
199 sample type, and segmented samples by symptom severity (**Fig. S6**). Indeed, the
200 bacterial abundance and composition in different sample types generally reflects disease
201 severity. In particular pharyngeal swab samples show a statistically significant difference
202 in bacterial ratio and species richness when comparing critical patients ("critical" group)
203 with non-critical patients ("mild", "moderate", and "severe" groups) (**Fig. 2C**). The
204 Shannon Diversity Index, however, is similar for all disease severities, indicating that
205 although the overall bacterial abundance is reduced in critical patients, the relative
206 abundance of different species remains stable. Interestingly, this phenomenon appears
207 to also correlated with patient age – In elderly patients above the age of 60, both bacterial
208 ratio and species richness are significantly reduced in critical patients as compared to

209 non-critical; this trend is not observed in patients younger than 60 years of age (**Fig S6**).
210 To further assess the relationship between bacterial metagenomic composition and
211 disease severity, we calculated the pairwise Bray-Curtis similarity for pharyngeal swab
212 samples, and found that mild, moderate, and severe patient samples are clustered
213 together and intermixed, while critical samples cluster separately with each other (**Fig.**
214 **2D**). The bacterial metagenomic composition is similar among critical patients and
215 suggests that they share common features distinct from non-critical patients. In light of
216 recent studies of the role of host immunity responses in critically ill COVID-19 patients[11-
217 14], our observations of the metagenomic signature could be indicative of the systemic
218 impact of the host immune response on commensal microbes, fungi, and other viruses in
219 the body. Currently, the number of critical patient samples in the younger group is limited,
220 but the trend is worth further investigation as more samples are collected over time.
221
222 In addition to the bacterial metagenomic signature, we also assessed the association
223 between viral composition and disease severity, and found a different trend presented in
224 the viral component. While bacterial abundances are reduced in critical patients as
225 compared to non-critical patients, viral abundances in critical patients are higher than in
226 non-critical patients (**Fig. 2E and S7**). Also different from the bacterial signature, the viral
227 species richness does not significantly change, but the Shannon diversity of viral species
228 in critical patients is significantly lower (**Fig. 2E**). This effect is partly contributed by a
229 greater abundance of SARS-Cov-2 sequences, which could then lead to a lower Shannon
230 Index as signals from low abundance viruses could be drowned out. Intriguingly, several
231 other viral families display increased abundance in critical patients as compared to non-
232 critical (**Fig. 2F**), including many dsDNA viruses that are known to establish latency such
233 as herpesviruses and papillomaviruses. One speculation is that the correlation of
234 abundance of these viral families with disease severity could be due to reactivation of
235 latent viruses under immunosuppressive medication, changes in host immune activity, or
236 direct SARS-CoV-2 activity[15-17]. The effect of age that we observed for bacteria is less
237 pronounced in viruses (**Fig. S8**), and is only observed for some viral families. Additional
238 sampling and deeper viral sequencing, as well as systematic experimental designs are
239 needed to further investigate these phenomena.

240

241 For severe viral pneumonia, co-infections can greatly affect patient outcomes[18-20]. One
242 recent study has showed that 50% of patients with COVID-19 who have died in this
243 pandemic had secondary bacterial infections[21]. By surveying the metagenomic landscape
244 of these samples, we observed several patient samples with exceptionally high
245 abundance of known pathogens, which could indicate a co-infection with SARS-Cov-2 in
246 those patients. We found ten cases of *S. aureus* and nine cases of *C. albicans* co-
247 infections, and the rate of co-infection for both pathogens is generally correlated with
248 disease severity (**Fig. 2G**).

249

250 **MINERVA achieves better SARS-CoV-2 genome coverage compared to**
251 **conventional dsDL strategies.** In both SHERRY and dsDL data, we detected low yet
252 significant levels of SARS-CoV-2 sequences. The viral ratio is between 10^{-7} and 10^{-1}. It is
253 worth noting that the SARS-CoV-2 sequence ratio is higher in SHERRY data than in dsDL
254 data (**Fig. 3A and 3B**), suggesting that SHERRY libraries capture more SARS-CoV-2
255 sequences. Though SARS-CoV-2 genome coverage and depth was not high in SHERRY
256 results due to low viral ratio and low sequencing depth, performing MINERVA
257 subsequently can enrich the SARS-CoV-2 sequence ratio up to 10,000-fold (**Fig. 3C and**
258 **S9**). As a result, MINERVA gives more complete and deeper coverage of SARS-CoV-2
259 genomes (**Fig. 3D and 3E**), despite sequencing dsDL libraries to two orders of magnitude
260 more depth (**Fig. S3**).

261

262 The superior quality of MINERVA data became clearer when we included clinical RT-
263 qPCR results. Both dsDL and MINERVA libraries detect SARS-CoV-2 sequences for
264 samples with various Ct values, but MINERVA produced more complete and deeper
265 genome coverage than dsDL methods (**Fig. 3F and 3G**), and this advantage is more
266 pronounced for low viral load samples, including two samples with negative qPCR results,
267 and stool samples. By studying the relationship between SARS-CoV-2 qPCR results and
268 read ratio, we identified two groups of samples that resulted in low SARS-CoV-2 genome
269 coverage when processed using dsDL (**Fig. 3H**). The first group had low SARS-CoV-2
270 read ratio, which prohibited the acquisition of enough SARS-CoV-2 sequencing reads.

The second group, which included most stool samples, had relatively high SARS-CoV-2 Ct values and read ratio, suggesting these samples had low total nucleic acid amount. Since dsDL approaches are less sensitive and require more input, this may explain why MINERVA outperforms dsDL most evidently in stool samples.

MINERVA can facilitate multiple facets of COVID-19 research. As a novel virus, little is known about the evolutionary features of SARS-CoV-2. Using 143 samples, we constructed a SARS-CoV-2 mutational profile (**Fig. 4A**), which was distinct from the Guangdong profile[22]. A few mutation sites, including the two linked to S and L strains[23], were found in multiple samples. Aided by the deep genome coverage in MIVERVA data, we not only detected strong linkage between position 8,782 and 28,144, but also observed high concordance of allele frequencies between these two positions. Furthermore, we detected strong linkage and high allele frequency concordance among four other positions, 241, 3,037, 14,408 and 23,403. Such allele frequency information offers additional layers of evidence supporting co-evolution of positions within the SARS-CoV-2 genome, in two distinct groups of samples. It is worth noting that in some samples, not all linked alleles are simultaneously detected, due to low coverage at some positions in those samples; these alleles can indeed be observed at low coverage in the raw data for these samples, but is missing from the post-processing data as they do not pass the stringent quality filtering steps. Nonetheless, the linkage was established by observing such linkage over many samples.

Several studies have examined the distribution of SARS-CoV-2 across different organs and tissues[7]. However, the presence of SARS-CoV-2 in the reproductive system is still under debate[24,25]. Aided by the high sensitivity of MINERVA, we detected a high abundance of SARS-CoV-2 sequences in semen samples from COVID-19 patients (**Fig. 4B**); several semen samples also had high SARS-CoV-2 genome coverage. SARS-CoV-2 SNV analysis demonstrated high similarity between semen and non-semen results (**Fig. 4C**).

Apart from its high infectiousness, the containment of SARS-CoV-2 transmission is

302 challenging due to the existence of asymptomatic infected individuals[26]. Though RT-
303 qPCR can be used to identify these individuals, elucidation of the chain of transmission
304 requires the complete SARS-CoV-2 sequences. To evaluate the performance of
305 MINERVA for tracking SARS-CoV-2 transmission, we sequenced the samples of several
306 asymptomatic individuals and their infected family members. SARS-CoV-2 SNV analysis
307 revealed that asymptomatic individuals each harbor viral sequences with unique
308 signatures, however, these individuals are clustered by the viral SNV signature with their
309 respective family members rather than other asymptomatic individuals, which indicates
310 that viral SNVs within infected families are similar to each other and unique from other
311 families (**Fig. 4D**). Summarily, despite the asymptomatic phenotype of some infected
312 individuals, the viral SNV signature generated by MINERVA can be used to accurately
313 place these individuals in the chain of transmission, enabling better epidemiological
314 tracking.
315
316 Recent studies have identified genetic variations of SARS-CoV-2 and raised the
317 possibility that multiple variants could co-exist in the same host individual. The intra-host
318 SNVs (iSNVs) detected in many samples (**Fig. 4A**) suggest that SARS-CoV-2 is rapidly
319 evolving within the hosts[2]. Through longitudinal sampling, we confirmed that iSNVs were
320 generally relatively stable across time and body sites (**Fig. S10**), but found that some
321 patients harbored greater variations in iSNVs (**Fig. 4E**). For P40 and P41, iSNVs were
322 stable within the same sample type across time, but varied across different sample types.
323 Comparing the two semen samples from Patient 152, changes in iSNV were clearly
324 observed. These results support the co-existence of multiple SARS-CoV-2 variants in the
325 same individual, and further investigation is warranted to understand this phenomenon.
326
327 In summary, MINERVA effectively converts metagenomes and SARS-CoV-2 sequences
328 into sequencing libraries with a simple and quick experimental pipeline, and subsequent
329 target enrichment can further improve SARS-CoV-2 genome coverage and genetic
330 variation detection. MINERVA can facilitate the study of SARS-CoV-2 genetics, and be
331 easily implemented to fight future RNA pathogen outbreaks.
332

Discussion

As of today, our knowledge of SARS-CoV-2 is still preliminary and much of it extrapolated from past studies of other beta coronaviruses such as SARS and MERS. However, the epidemiology, physiology, and biology of COVID-19 are evidently unique[27]. To speed up our investigation of this virus and the disease it causes, a practical protocol for viral genome research of clinical samples is urgently needed. Currently, methods for transforming clinical samples into sequencing libraries are laborious and painstaking, while clinical personnel at the frontlines are already strained for time and energy. MINERVA minimizes the need for expert technique and hands-on operation; we believe it will be pivotal in accelerating clinical research of SARS-CoV-2.

Recent evolutionary tracing studies suggest the emergence of multiple novel, evolved subtypes of SARS-CoV-2[28], including the S/L-subtypes[23] and the A/B/C-variants[29]. New variants will likely continue to emerge as the virus mutates, and to uncover them requires deep, complete coverage of viral genomes from a large number of patients. With the existence of asymptomatic carriers[26] and possible recurrent infections in the same individual[30], longitudinal re-sampling of patients is also important to uncover intra-host viral heterogeneity, but as viral load decreases with time[31], the sensitivity of the sample processing method becomes critical. These studies all require processing large volumes of clinical samples with a highly robust and scalable method that does not compromise on sensitivity. We have demonstrated that MINERVA libraries from clinical samples can generate deep and complete coverage of SARS-CoV-2 genomes that can be used for evolutionary tracing and variant characterization research. Furthermore, the high sensitivity, high coverage, and high depth of the SARS-CoV-2 viral genomes obtained by MINERVA can reveal unique viral SNV signatures in each patient, even if they are asymptomatic. We showed that these viral SNVs allows families of infected individuals to be co-clustered, but are unique between families, which enables each individual to be accurately placed in the chain of transmission. As MINERVA is easily scalable and implementable in a clinical lab setting, it can serve as a robust strategy for timely and critical epidemiological tracking and monitoring during a pandemic.

364 It is well-established now that SARS-CoV-2 can infect multiple organ systems, tissue
365 compartments, and cell types[2,7,32,33]. In our profiling of COVID-19 clinical samples from
366 multiple body sites of the same patient, we found that the viral load and viral subtypes
367 vary across different body sites, possibly affected by interactions between microbial and
368 other viral species as well as overall metagenomic diversity present in different
369 microenvironments of each body site. The effects of metagenomic diversity and inter-
370 compartment heterogeneity on SARS-CoV-2 biology and COVID-19 symptom severity
371 are also not understood. In particular, it is difficult to obtain high-quality unbiased
372 metagenomic using conventional library construction methods from low-quantity samples,
373 as well as samples such as stool in which bacteria dominate the metagenomes, as
374 conventional methods are not sufficiently sensitive. The versatility of MINERVA as a two-
375 part protocol integrating a tailored SHERRY and post-library virus enrichment provides
376 flexibility for sample processing that uses one standard sample pipeline for both highly
377 sensitive metagenomic analysis and targeted deep sequencing of specific transcripts.
378 Using MINERVA, we have demonstrated the first large scale profiling of metagenomic
379 composition of different body sites in the context of COVID-19. One pre-print study
380 investigated the relationship between gut microbes and COVID-19 severity, and
381 purportedly found links between gut microbe composition with blood proteomic
382 biomarkers that predict symptom severity[34], however, there is no discussion of
383 metagenomic composition of other body sites. As we show here with MINERVA data from
384 a wide range of sample types, there are large body site-specific differences, and our data
385 suggests that microbial and viral metagenomic composition in pharyngeal swab samples
386 also significantly correlates with disease severity. The metagenomic profile of these other
387 body sites that are arguably more directly involved in the viral infection, have not been
388 reported or investigated elsewhere. Using MINERVA we highlight several new directions
389 of clinical and basic research, and with further investigation, these could shed light on the
390 complex interactions between SARS-CoV-2 pathology, host microbial communities, host
391 immunity, and disease progression. We also showed that MINERVA metagenomic profiles
392 can identify potential co-infections of bacteria, fungi, and other viruses, which is
393 challenging to do with conventional approaches. In our samples, we found a co-infection
394 rate of ~ 20% (16/79 patients), which is higher than the rate reported by one secondary

395 study of COVID-19 co-infections[35]. In this secondary study, although they found 8% of
396 patients experiencing bacterial/fungal co-infection, the rate of broad spectrum antibiotic
397 use for COVID-19 patients is much higher (72%). It is well-known that co-infections in
398 severe pneumonia can greatly affect patient outcomes[19,20], and it is estimated that 50%
399 of patients with COVID-19 who have died in this pandemic had secondary bacterial
400 infections[21]. Our result shows the utility of MINERVA in identifying non-viral co-infections,
401 and further primary studies using MINERVA could help to elucidate true co-infection rates
402 to guide better strategies for antibiotic use.
403
404 MINERVA was not created to be a rapid diagnostic assay; rather, we hope its ease-of-
405 use, versatility, scalability, sensitivity, and cost-effectiveness will drive adoption of routine
406 sequencing of COVID-19 clinical samples, and thereby facilitate multiple areas of much-
407 needed SARS-CoV-2 and COVID-19 research for clinicians and researchers.
408
409
410 **Author contributions**
411 C.C., Y.C., X.S.X., H.Z., Y.H. and J.W. conceived the project; J.L., P.D., Q.L. and C.S.
412 conducted experiments; C.C., L.D., Q.J., J.L., Y.H. and J.W. analyzed the data; C.C., J.L.,
413 L.D., Q.J., A.R.W., Y.H. and J.W. wrote the manuscript with the help from all other authors.
414
415 **Conflict of interest statement**
416 The authors declare no conflict of interest.
417
418 **Acknowledgement**
419 We thank Ms. Chenyang Geng and BIOPIC sequencing platform at Peking University for
420 the assistance of high-throughput sequencing experiments, and Ms. Amelia Huang for
421 the assistance of figure preparation. This work was supported by National Natural
422 Science Foundation of China (21675098, 21927802, 21525521), Ministry of Science and
423 Technology of China (2018YFA0800200, 2018YFA0108100, 2018YFC1002300), 2018
424 Beijing Brain Initiation (Z181100001518004), Beijing Advanced Innovation Center for
425 Structural Biology, Beijing Advanced Innovation Center for Genomics, HKUST's start-up

and initiation grants (Hong Kong University Grants Committee), Hong Kong Research Grants Council Theme-based Research Scheme (RGC TBRS T12-704/16R-2) and Collaborative Research Fund (RGC CRF C6002-17G), Hong Kong RGC Early Career Support Scheme (RGC ECS 26101016), Hong Kong Epigenomics Project (LKCCFL18SC01-E), and HKUST BDBI Labs.

Reference

1. WHO Coronavirus Disease (COVID-19) Dashboard (covid19.who.int)
2. Wölfel, R. *et al.* Virological assessment of hospitalized patients with COVID-2019. *Nature* Online Publication (2020). doi:10.1038/s41586-020-2196-x
3. Ren, L.-L. *et al.* Identification of a novel coronavirus causing severe pneumonia in human. *Chinese Medical Journal* Online Publication (2020). doi: 10.1097/CM9.0000000000000722
4. Lu, R. *et al.* Genomic characterisation and epidemiology of 2019 novel coronavirus: implications for virus origins and receptor binding. *Lancet* 395, 565–574 (2020). doi: 10.1016/S0140-6736(20)30251-8
5. Zhou, P. *et al.* A pneumonia outbreak associated with a new coronavirus of probable bat origin. *Nature* Online Publication (2020). doi:10.1038/s41586-020-2012-7
6. Wu, F. *et al.* A new coronavirus associated with human respiratory disease in China. *Nature* Online Publication (2020). doi:10.1038/s41586-020-2008-3
7. Wang, W. *et al.* Detection of SARS-CoV-2 in Different Types of Clinical Specimens. *JAMA* Online Publication (2020). doi:10.1001/jama.2020.3786
8. Deng, X. *et al.* A Genomic Survey of SARS-CoV-2 Reveals Multiple Introductions into Northern California without a Predominant Lineage. *medRxiv* Online Publication (2020). doi:10.1101/2020.03.27.20044925
9. Xiao, M. *et al.* Multiple approaches for massively parallel sequencing of HCoV-19 (SARS-CoV-2) genomes directly from clinical samples. *bioRxiv* Online Publication (2020). doi:10.1101/2020.03.16.993584
10. Di, L. *et al.* RNA sequencing by direct tagmentation of RNA/DNA hybrids. *Proceedings of the National Academy of Sciences of the United States of America* 117, 2886–2893 (2020). doi: 10.1073/pnas.1919800117
11. Jose, R. J. & Manuel, A. COVID-19 cytokine storm: the interplay between inflammation and coagulation. *The Lancet Respiratory* Online Publication (2020). doi:10.1016/S2213-2600(20)30216-2
12. Giamarellos-Bourboulis, E. J. *et al.* Complex Immune Dysregulation in COVID-19 Patients with Severe Respiratory Failure. *Cell Host & Microbe* Online Publication (2020). doi:10.1016/j.chom.2020.04.009

464 13. Wang, F. *et al.* The laboratory tests and host immunity of COVID-19 patients with
465 different severity of illness. *JCI Insight* 5, 531–12 (2020).
466 doi:10.1172/jci.insight.137799

467 14. Tay, M. Z., Poh, C. M., nia, L. R. X., MacAry, P. A. & Ng, L. F. P. The trinity of
468 COVID-19: immunity, inflammation and intervention. *Nat. Rev. Immunol.* Online
469 Publication (2020). doi:10.1038/s41577-020-0311-8

470 15. Stoeger, T. & Adler, H. 'Novel' Triggers of Herpesvirus Reactivation and Their
471 Potential Health Relevance. *Front. Microbiol.* 9, 229–4 (2019).doi:
472 10.3389/fmicb.2018.03207

473 16. Maglennon, G. A., McIntosh, P. B. & Doorbar, J. Immunosuppression Facilitates
474 the Reactivation of Latent Papillomavirus Infections. *Journal of Virology* 88, 710–
475 716 (2013). doi:10.1128/JVI.02589-13

476 17. Ritchie, A. I. & Singanayagam, A. Immunosuppression for hyperinflammation in
477 COVID-19: a double-edged sword? *The Lancet* 395, 1111 (2020).
478 doi:10.1016/S0140-6736(20)30691-7

479 18. Cox, M. J., Loman, N., Bogaert, D. & O'Grady, J. Co-infections: potentially lethal
480 and unexplored in COVID-19. *The Lancet Microbe* Online Publication, e11 (2020).

481 19. Crotty, M. P. *et al.* Epidemiology, Co-Infections, and Outcomes of Viral
482 Pneumonia in Adults. *Medicine* 94, e2332–6 (2015).
483 doi:10.1126/scitranslmed.aan1589

484 20. Shah, N. S. *et al.* Bacterial and viral co-infections complicating severe influenza:
485 Incidence and impact among 507 U.S. patients, 2013–14. *Journal of Clinical*
486 *Virology* 80, 12–19 (2016). doi:10.1016/j.jcv.2016.04.008

487 21. Zhou, F. *et al.* Clinical course and risk factors for mortality of adult inpatients with
488 COVID-19 in Wuhan, China: a retrospective cohort study. *The Lancet* 395, 1054–
489 1062 (2020). doi: 10.1016/S0140-6736(20)30566-3

490 22. Lu, J. *et al.* Genomic epidemiology of SARS-CoV-2 in Guangdong Province,
491 China. *Cell* Online Publication (2020). doi:10.1016/j.cell.2020.04.023

492 23. Tang, X. *et al.* On the origin and continuing evolution of SARS-CoV-2. *National*
493 *Science Review* Online Publication (2020). doi:10.1093/nsr/nwaa036

494 24. Pan, F. *et al.* No evidence of SARS-CoV-2 in semen of males recovering from
495 COVID-19. *Fertility and Sterility* Online Publication (2020).
496 doi:10.1016/j.fertnstert.2020.04.024

497 25. Li, D., Jin, M., Bao, P., Zhao, W. & Zhang, S. Clinical Characteristics and Results
498 of Semen Tests Among Men With Coronavirus Disease 2019. *JAMA Netw Open*
499 3, e208292–3 (2020). doi: 10.1001/jamanetworkopen.2020.8292

500 26. Bai, Y. *et al.* Presumed Asymptomatic Carrier Transmission of COVID-19. *JAMA*
501 323, 1406–1407 (2020). doi: 10.1001/jama.2020.2565

502 27. Fauci, A. S., Lane, H. C. & Redfield, R. R. Covid-19 — Navigating the Uncharted.
503 *N Engl J Med* 382, 1268–1269 (2020). doi: 10.1056/NEJMe2002387

28. Gudbjartsson, D. F. *et al.* Spread of SARS-CoV-2 in the Icelandic Population. *N Engl J Med* Online Publication (2020). doi:10.1056/NEJMoa2006100

29. Forster, P., Forster, L., Renfrew, C. & Forster, M. Phylogenetic network analysis of SARS-CoV-2 genomes. *PNAS* Online Publication (2020). doi: 10.1073/pnas.2004999117

30. An, J. *et al.* Clinical characteristics of the recovered COVID-19 patients with re-detectable positive RNA test. *medRxiv* Online Publication (2020). doi:10.1101/2020.03.26.20044222

31. He, X. *et al.* Temporal dynamics in viral shedding and transmissibility of COVID-19. *Nature Medicine* Online Publication (2020). doi:10.1038/s41591-020-0869-5

32. Young, B. E. *et al.* Epidemiologic Features and Clinical Course of Patients Infected With SARS-CoV-2 in Singapore. *JAMA* 323, 1488–1494 (2020). doi: 10.1001/jama.2020.3204

33. SARS-CoV-2–Positive Sputum and Feces After Conversion of Pharyngeal Samples in Patients With COVID-19. *Annals of Internal Medicine* Online Publication (2020). doi: 10.7326/M20-0991

34. Gou, W. *et al.* Gut microbiota may underlie the predisposition of healthy individuals to COVID-19. *medRxiv* Online Publication (2020). doi:10.1101/2020.04.22.20076091

35. Rawson, T. M. *et al.* Bacterial and fungal co-infection in individuals with coronavirus: A rapid review to support COVID-19 antimicrobial prescribing. *Clin Infect Dis.* Online Publication (2020). doi:10.1093/cid/ciaa530

529 **Figure Caption**

530

531 **Figure 1. Scheme and optimization of MINERVA.** (A) RNA extracted from pharyngeal
532 swabs, sputum and stool samples undergo rRNA and DNA removal before a SHERRY
533 processing pipeline metagenomic sequencing library construction. Multiple libraries were
534 then pooled for SARS-CoV-2 sequence enrichment. (B) COVID-19 sample profiles,
535 showing the age group, sex, severity, and re-sampling status of each patient. (C) Effect
536 of sample input and reaction volume on sequencing depth of SARS-CoV-2 genome. (D)
537 Metagenomic results of carrier RNA removal tests. (E) SARS-CoV-2 results of carrier RNA
538 removal test.

539

540 **Figure 2. Metagenomic analyses of different sample types using MINERVA.** (A) PCA
541 analysis of bacterial composition in different sample types reveal body site-specific
542 features. PCA analysis is based on bacterial genus of different sample types (60
543 pharyngeal, 51 sputum, and 25 stool samples). The bacterial genus composition of
544 pharyngeal and sputum samples are more similar to each other, while stool samples are
545 distinct from all other sample types. (B) Clustering analysis of bacterial composition in
546 different sample types reveals characteristic microbial features in patients with the most
547 severe disease symptoms. Bacteroides was dominant in stool samples while in oral
548 samples (pharyngeal and sputum), samples from critical patients can be easily
549 distinguished from patients with lower disease severity by the low abundance of
550 Streptococcus and Rothia, and the high abundance of Pseudomonas. (C) Bacterial
551 abundance and composition in pharyngeal swab samples significantly distinguish
552 between critical and non-critical patients. Comparison of bacterial ratio and within-subject
553 diversity between critical (n=42) and non-critical (n=18) pharyngeal samples. The
554 bacterial ratio and species richness were significantly lower in Critical patients compared
555 with non-Critical patients, while the Shannon index of alpha diversity is slightly higher,
556 though not significant (Mann-Whitney U test). (D) Bacterial metagenomic composition is
557 similar among critical patient samples and distinct from non-critical patient samples. Bray-
558 Curtis beta diversity among all pharyngeal samples (n=60) at different stages. Severity
559 samples were distinct from other stages. (E) Viral abundance correlates with disease

560 severity. Comparison of viral ratio and within-subject diversity between critical samples
561 (n=42) and non-critical pharyngeal samples (n=18). The viral ratio was significant higher
562 in critical samples, while the species richness and Shannon index was slightly lower
563 (Mann-Whitney U test). (F) Certain viral families correlate strongly with disease severity.
564 Comparison of SARS-Cov-2 and other viral family relative abundance between critical
565 (n=42) and non-critical (n=18) pharyngeal samples. The relative abundance of SARS-
566 Cov-2, Coronaviridae, Herpesviridae, Papillomaviridae and Poxviridae were significantly
567 higher in Critical samples (Mann-Whitney U test). (G) Metagenomic analysis of SHERRY
568 libraries detect potential co-infection in specific patient samples. The cutoff of relative
569 abundance for infection detection was set to 1% to avoid potential false positives. Higher
570 rate of Staphylococcus aureus and Candida albicans can be detected in critical patients.
571
572 **Figure 3. Direct comparison between sequencing libraries constructed from**
573 **MINERVA and conventional dsDL strategies.** (A) SARS-CoV-2 mapping ratio statistics
574 of SHERRY and dsDL libraries. (B) Comparison of SARS-CoV-2 mapping ratios between
575 SHERRY and dsDL libraries. (C) Comparison of SARS-CoV-2 mapping ratios between
576 SHERRY and MINERVA libraries. (D and E) SARS-CoV-2 genome coverage and depth
577 statistics of MINERVA and dsDL libraries. (F and G) Comparison of SARS-CoV-2
578 sequencing results between MINERVA and dsDL libraries. (H) Metagenomic sequencing
579 and qPCR result features of samples with poor SARS-CoV-2 genome coverage.
580
581 **Figure 4. MINERVA could facilitate COVID-19 and SARS-CoV-2 research through**
582 **accurate and sensitive identification of viral mutations.** (A) SARS-CoV-2 mutation
583 profile obtained from 101 samples. (B) SARS-CoV-2 genome coverage of semen samples
584 and other types of samples from the same patients. (C) SARS-CoV-2 mutations in semen
585 and stool samples from Patient 112. (D) SARS-CoV-2 mutation profiles of asymptomatic
586 patients and their infected family members. (E) Longitudinal SARS-CoV-2 mutation
587 analysis of individual patients.
588
589 **Figure S1**. Comparison of workflow between MINERVA and the conventional dsDL
590 strategy.

591

592 **Figure S2**. Optimization of SHERRY protocol. (A-C) Effect of N10 primer during reserve
593 transcription and Tn5 amount on detected gene number, ribosomal rate and insert size.
594 (D-F) Effect of N10 primer during reserve transcription and Tn5 amount on gene body
595 coverage evenness.

596

597 **Figure S3**. Amount of sequencing data for different libraries.

598

599 **Figure S4**. Comparison between SHERRY and dsDL libraries on total viral ratio (A), total
600 fungal ratio (B), total bacterial ratio (C), and bacterial entropy (D).

601

602 **Figure S5**. PCA analysis of viral and fungal compositions in different sample types. (A)
603 Viral family composition in all samples. The viral composition of faeces samples was
604 distinct from oral samples. (B) Fungal family composition in all samples. There is no major
605 difference among different sample types and stages. While *Candida* can be detected with
606 high level in certain patients.

607

608 **Figure S6**. Bacterial composition by severity in different sample types and age groups.
609 (A) Bacterial composition by severity in different sample types. The severity stage is highly
610 related to age. The bacterial ratio and species richness were significantly lower in critical
611 pharyngeal samples (Kruskal-Wallis test and Dunn's post-hoc test). This was not
612 observed in sputum samples may be because of the small sample size. (In pharyngeal
613 samples, mild=15, moderate=19, severe=8, critical=18; while in sputum samples, mild=8,
614 moderate=34, severe=8, critical=1). (B) Comparison of bacterial ratio and within-subject
615 diversity between non-critical (n=8) and critical patients (n=16) in old group (>=60 years
616 old) to avoid the bias from age. The bacterial ratio and species richness were lower in
617 critical patients while the Shannon index is higher (Mann-Whitney U test). (C) Comparison
618 of bacterial ratio and within-subject diversity between critical (n=2) and non-critical
619 patients (n=34) in young group (<60 years old). The bacterial ratio and species richness
620 were lower in critical patients while the Shannon index is higher.

621

622 **Figure S7**. Viral composition by severity in different sample types. The viral ratio was
623 significantly lower in critical patients compared to other patients in pharyngeal samples
624 (Kruskal-Wallis test and Dunn's post-hoc test).
625
626 **Figure S8**. Bacterial composition by severity in different age groups. (A) Comparison of
627 relative abundance of SARS-Cov-2 and Coronovaridae between non-critical (n=8) and
628 critical (n=16) old (>=60) patients in pharyngeal samples. Critical patients have higher
629 level of SARS-Cov-2 and Coronaviridae (Mann-Whitney U test). (B) Comparison of
630 relative abundance of SARS-Cov-2 and Cronovaridae between non-critical (n=34) and
631 critical (n=2) young (<60) patients in pharyngeal samples. Critical patients have higher
632 level of SARS-Cov-2 and Coronaviridae (Mann-Whitney U test). (C) Comparison of
633 relative abundance of Herpesviridae, Papillomaviridae and Poxviridae between non-
634 critical (n=8) and critical (n=16) old (>=60) patients in pharyngeal samples. The
635 abundance of these three viral families was higher in Critical patients (Mann-Whitney U
636 test). (D) Comparison of relative abundance of Herpesviridae, Papillomaviridae and
637 Poxviridae between non-critical (n=8) and critical (n=16) young (<60) patients in
638 pharyngeal samples. The abundance of these three viral families was higher in Critical
639 patients (Mann-Whitney U test).
640
641 **Figure S9**. SARS-CoV-2 genome sequencing results of SHERRY and MINERVA libraries.
642 (A) SARS-CoV-2 mapping ratio statistics of MINERVA libraries. (B and C) SARS-CoV-2
643 genome coverage and depth statistics of SHERRY libraries.
644
645 **Figure S10**. Longitudinal SARS-CoV-2 mutation analysis of individual patients.
646

647 **Material and Methods**

648

649 **Ethics approval**

650 This study was approved by the Ethics Committee of Beijing Ditan Hospital, Capital
651 Medical University (No. KT2020-006-01).

652

653 **Optimization of SHERRY protocol**

654 We used the total RNA extracted from 3T3 cells to optimize experimental protocols. RNA
655 extraction was performed using RNeasy Mini Kit (Qiagen, Cat.No.74104). DNA was then
656 removed through DNase I (NEB, Cat.No.M0303) digestion. The resulting total RNA was
657 concentrated by RNA Clean & Concentrator-5 kit (Zymo Research, Cat R1015), and its
658 quality was assessed by the Fragment Analyzer Automated CE System (AATI). Its
659 quantification was done by Qubit 2.0 (Invitrogen). To optimize the SHERRY protocol,
660 different amount of random decamer (N10) (0, 10, or 100 pmol) was used to set up
661 reverse transcription reactions. Titration of Tn5 transposome (0.2, 0.5, or 1.0 μl Vazyme
662 V50; 0.05 or 0.25 μl home-made pTXB1) was performed in tagmentation procedure. In
663 all tests, 10 ng 3T3 total RNA was used, and all reagents except for N10 or Tn5
664 transposome remain unchanged. All libraries were sequenced on Illumina NextSeq 500
665 with 2x75 paired-end mode. Clean data was aligned to GRCm38 genome and known
666 transcript annotation using Tophat2 v2.1.1. Ribosome-removed aligned reads were
667 proceeded to calculate FPKM by Cufflinks v2.2.1 and gene body coverage by RSeQC
668 v.2.6.4.

669

670 **Patients and clinical samples**

671 From January 23, 2020 to April 20, 2020, 91 patients were enrolled in this study according
672 to the 7th guideline for the diagnosis and treatment of COVID-19 from the National Health
673 Commission of the People's Republic of China. All patients, diagnosed with COVID-19,
674 were hospitalized in Beijing Ditan Hospital and classified into four severity degrees, mild,
675 moderate, severe, and critical illness, according to the guideline. We collected 143
676 samples (60 pharyngeal swabs, 52 sputum samples, 25 stool samples, and 6 semen
677 samples) from these patients.

678

679 **RNA extraction and rRNA removal**

680 For all the clinical samples, nucleic acids extraction was performed in a BSL-3 laboratory.
681 Samples were deactivated by heating at 56°C for 30 min before extraction. Total RNA
682 was extracted using QIAamp Viral RNA Mini Kit (Qiagen) following the manufacturer's
683 instructions. In most samples (79 out of 85) we specifically omitted the use of carrier RNA
684 due to its interference on the most prevalent sample preparation protocols for high-
685 throughput sequencing. After nucleic acids extraction, rRNA was removed by rDNA probe
686 hybridization and RNase H digestion, followed by DNA removal through DNase I digestion,
687 using MGIEasy rRNA removal kit (BGI, Shenzhen, China). The final elution volume was
688 12-20 µl for each sample. For carrier RNA removal tests, 1.7 µg polyA carrier RNA was
689 spiked into 18 µl of elute from QIAamp Viral RNA Mini Kit. To remove the carrier RNA from
690 these spike-in samples and other samples extracted with carrier RNA, 2 µg poly(T) 59-
691 mer (T59) oligo was added during the rDNA hybridization step.

692

693 **dsDL Metagenomic RNA library construction and sequencing**

694 The libraries were constructed using MGIEasy reagents (BGI, China) following
695 manufacture's instruction. The purified RNA, after rRNA depletion and DNA digestion,
696 underwent reverse transcription, second strand synthesis, and sequencing adaptor
697 ligation. After PCR amplification, DNA was denatured and circularized before being
698 sequenced on DNBSEQ-T7 sequencers (BGI, China).

699

700 **MINERVA library preparation**

701 Totally, 2.7 µl RNA from rRNA and DNA removal reaction was used for standard SHERRY
702 reverse transcription, with the following modifications: 1) 10 pmol random decamer (N10)
703 was added to improve coverage; 2) initial concentrations of dNTPs and oligo-dT (T30VN)
704 were increased to 25 mM and 100 µM, respectively. For 5.4 µl and 10.8 µl input, the entire
705 reaction was simply scaled up 2 and 4 folds, respectively. The RNA/DNA hybrid was
706 tagmented in TD reaction buffer (10 mM Tris-Cl pH 7.6, 5 mM $MgCl_2$, 10% DMF)
707 supplemented with 3.4% PEG8000 (VWR Life Science, Cat.No.97061), 1 mM ATP (NEB,
708 Cat.No. P0756), and 1U/µl RNase inhibitor (TaKaRa, Cat.No. 2313B). The reaction was

709 incubated at 55°C for 30 min. 20 µl tagmentation product was mixed with 20.4 µl Q5 High-
710 Fidelity 2X Master Mix (NEB, Cat.No. M0492L), 0.4 µl SuperScript II reverse transcriptase,
711 and incubated at 42°C for 15 min to fill the gaps, followed by 70°C for 15 min to inactivate
712 SuperScript II reverse transcriptase. Then index PCR was performed by adding 4 µl 10
713 µM unique dual index primers and 4 µl Q5 High-Fidelity 2X Master Mix, with the following
714 thermo profile: 98°C 30 s, 18 cycles of [98°C 20 s, 60°C 20 s, 72°C 2 min], 72°C 5 min.
715 The PCR product was then purified with 0.8x VAHTS DNA Clean Beads (Vazyme, Cat.
716 No. N411). These SHERRY libraries were sequenced on Illumina NextSeq 500 with 2x75
717 paired-end mode for metagenomic analysis.
718 For preparing MINERVA libraries through SARS-CoV-2 enrichment, 1µl SHERRY
719 metagenomic library was first quantified with N gene using quantitative PCR (F:
720 GGGGAACTTCTCCTGCTAGAAT, R: CAGACATTTTGCTCTCAAGCTG) after 1:200
721 dilution, then multiple libraries were pooled together based on qPCR results and
722 processed with TargetSeq One Cov Kit (iGeneTech, Cat.No.502002-V1) following
723 manufacturer's instruction. The iGeneTech Blocker was replaced by the IDT xGen
724 Universal Blockers (NXT). These MINERVA libraries were sequenced on Illumina
725 NextSeq 500 with 2x75 paired-end mode for deep SARS-CoV-2 analysis.
726
727 **Data processing**
728 For metagenomic RNA-seq data, raw reads were quality controlled using BBmap (version
729 38.68) and mapped to the human genome reference (GRCh38) using STAR (version
730 2.6.1d) with default parameters. All unmapped reads were collected using samtools
731 (version 1.3) for microbial taxonomy assignment by Centrifuge (version 1.0.4). Custom
732 reference was built from all complete bacterial, viral and any assembled fungal genomes
733 downloaded from NCBI RefSeq database (viral and fungal genomes were downloaded
734 on February 4th, 2020, and bacterial genomes were downloaded on November 14th,
735 2018). There were 11,174 bacterial, 8,997 viral, and 308 fungal genomes respectively.
736 Bacterial Shannon diversity (entropy) was calculated at species level, and the species
737 abundance was measured based on total reads assigned at the specific clade normalized
738 by genome size and sequencing depth. Bacterial genus composition was analyzed based
739 on reads proportion directly assigned by Centrifuge. For dsDL sequencing data, sub-

740 sampling was performed for each sample to obtain ~12M paired-end nonhuman reads,
741 which is the median of SHERRY datasets. Same workflow was performed as described
742 above for the removal of human reads and microbial taxonomy assignment.
743 For SARS-CoV-2 genome analysis, raw reads were trimmed to remove sequencing
744 adaptors and low-quality bases with Cutadapt v1.15. BWA 0.7.15-r1140 was used to align
745 reads to the SARS-CoV-2 reference genome (NC_045512.2). Then we removed
746 duplicates from the primary alignment with Picard Tools v2.17.6. We used mpileup
747 function in samtools v1.10 to call SNP and InDel with parameter -C 50 -Q 30 -q 15 -E -d
748 0. We called mutation if the depth >=10 and strand bias >0.25. The strand bias is defined
749 as the value that minimum of positive strand depth and negative strand depth divided by
750 the maximum.
751
752
753 **Data deposition**
754 The sequencing data generated during this study have been uploaded to Genome
755 Sequencing Archive (PRJCA002533). However, due to ethical concerns, access to the
756 datasets is only available from the corresponding author on reasonable request.
757
758
759
760

Figure 1

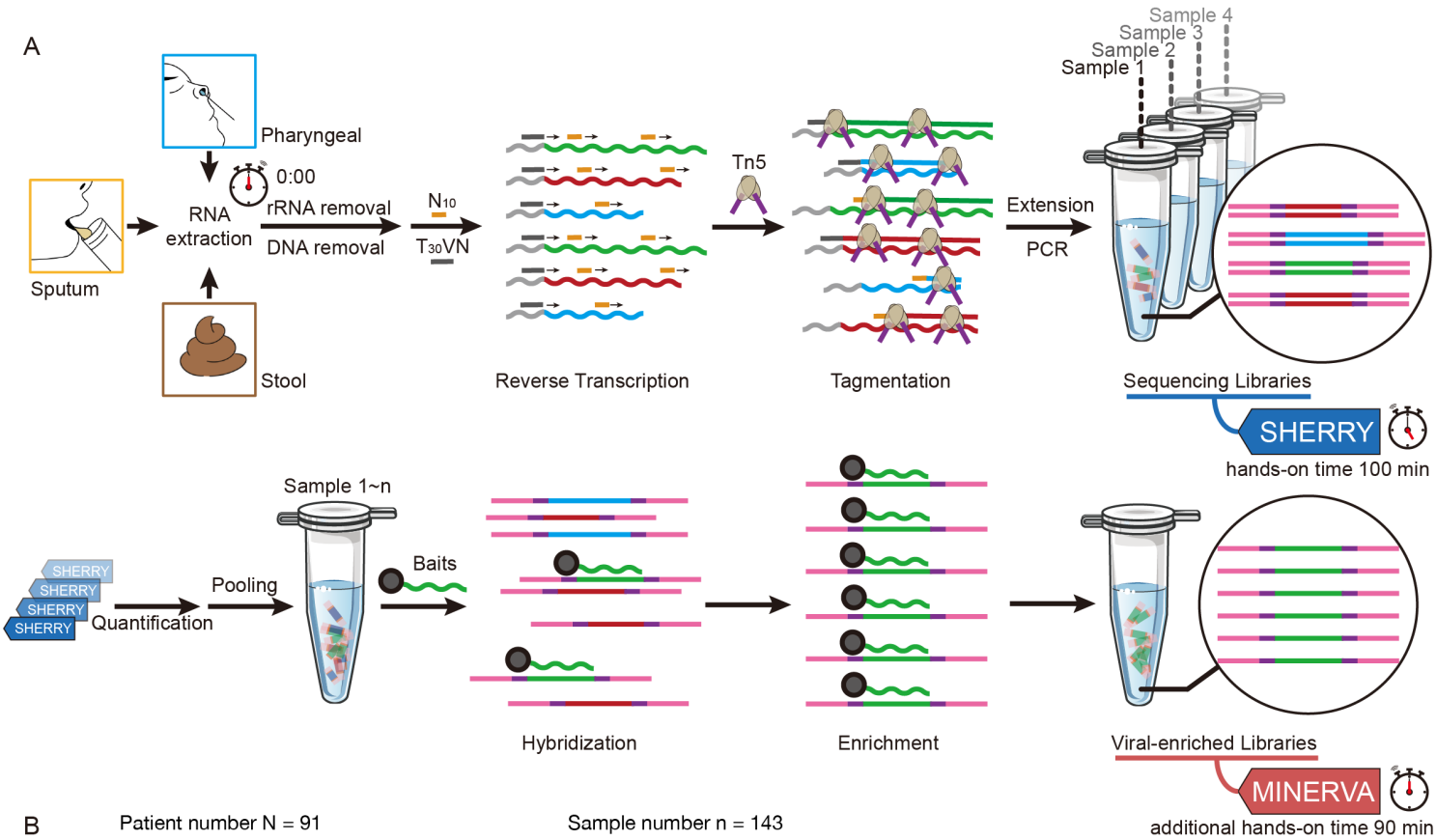
A
Pharyngeal
0:00
RNA extraction
rRNA removal
DNA removal
N10
T30VN
Sputum
Stool
Reverse Transcription
Tn5
Tagmentation
Extension
PCR
Sample 4
Sample 3
Sample 2
Sample 1
Sequencing Libraries
SHERRY
hands-on time 100 min
SHERRY
SHERRY
SHERRY
SHERRY
Quantification
Pooling
Sample 1~n
Baits
Hybridization
Enrichment
Viral-enriched Libraries
MINERVA
additional hands-on time 90 min

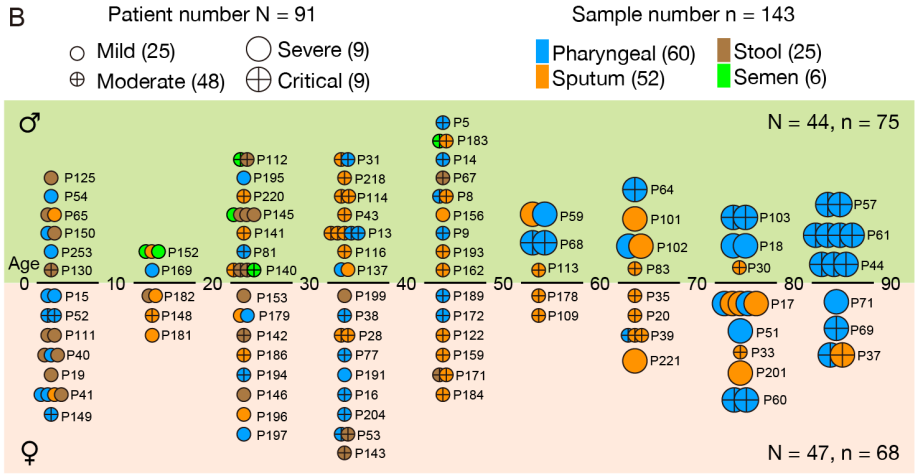
B
Patient number N = 91
Mild (25)
Severe (9)
Moderate (48)
Critical (9)
Sample number n = 143
Pharyngeal (60)
Stool (25)
Sputum (52)
Semen (6)
N = 44, n = 75
N = 47, n = 68
Age

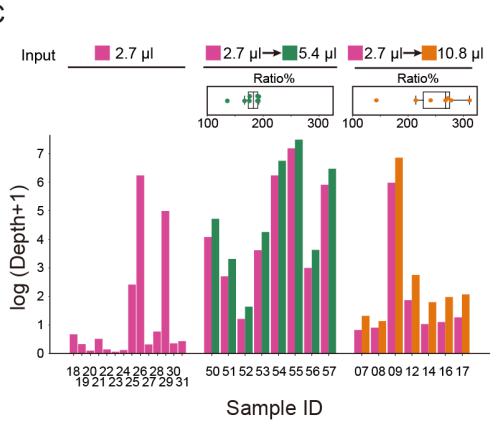
C
Input
2.7 µl
2.7 µl → 5.4 µl
2.7 µl → 10.8 µl
Ratio%
log (Depth+1)
Sample ID

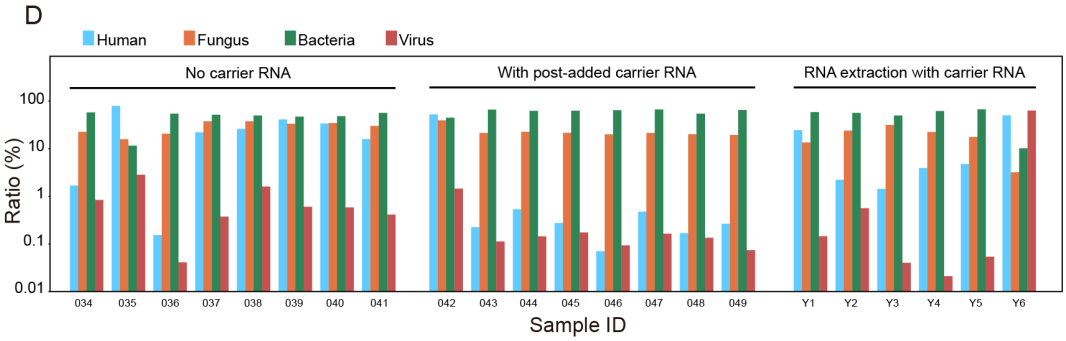
D
Human
Fungus
Bacteria
Virus
No carrier RNA
With post-added carrier RNA
RNA extraction with carrier RNA
Ratio (%)
Sample ID

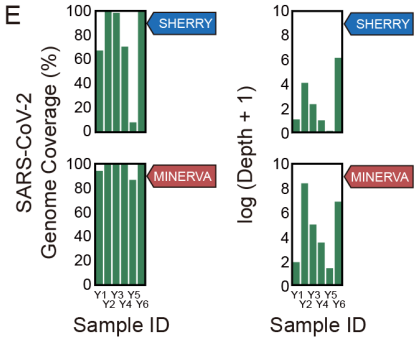
E
SARS-CoV-2 Genome Coverage (%)
SHERRY
MINERVA
log (Depth + 1)
Sample ID

Figure 2

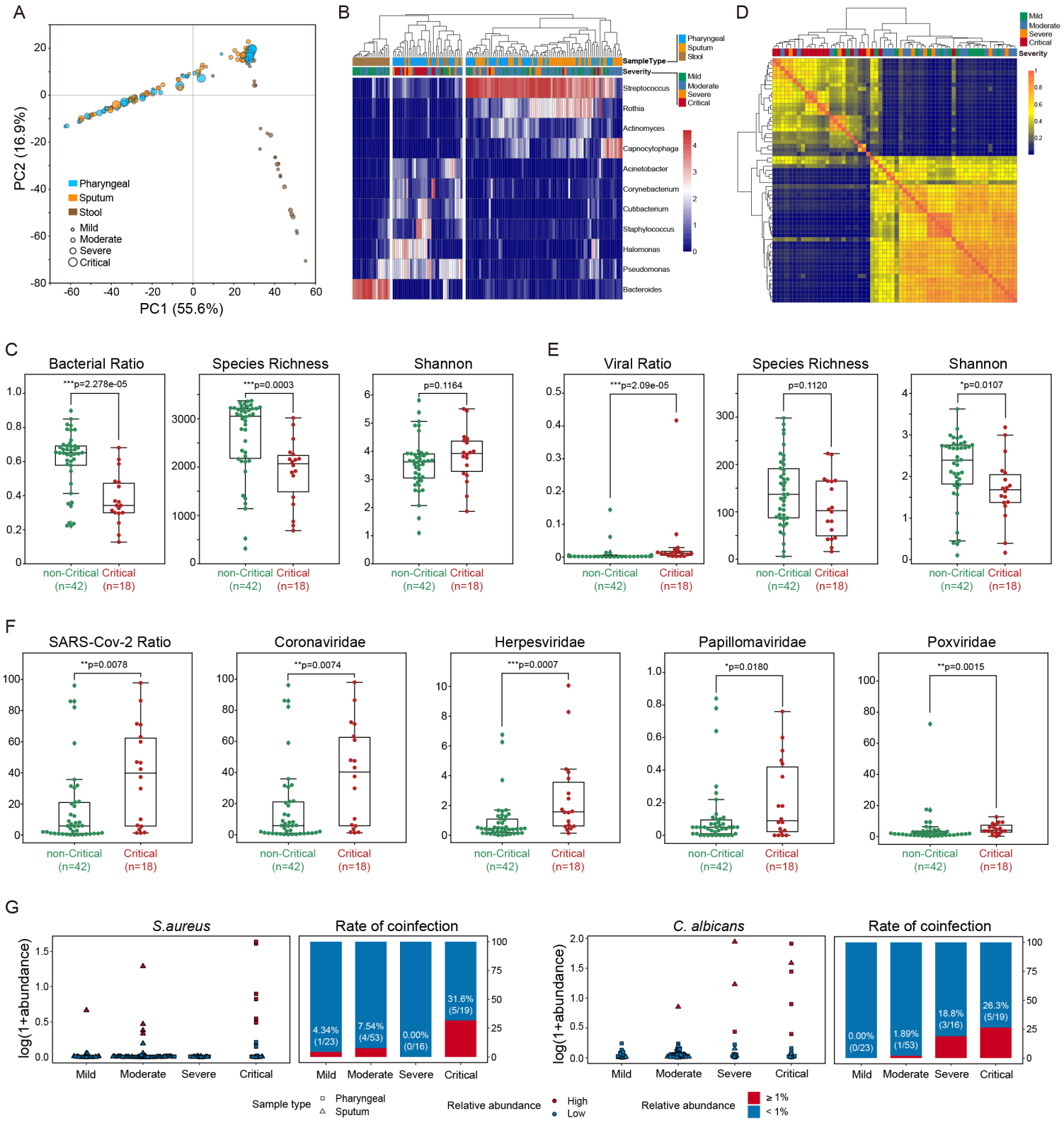
A
PC2 (16.9%)
PC1 (55.6%)
Pharyngeal
Sputum
Stool
Mild
Moderate
Severe
Critical
B
SampleType
Severity
Pharyngeal
Sputum
Stool
Mild
Moderate
Severe
Critical
Streptococcus
Rothia
Actinomyces
Capnocytophaga
Acinetobacter
Corynebacterium
Cutibacterium
Staphylococcus
Halomonas
Pseudomonas
Bacteroides
D
Mild
Moderate
Severe
Critical
Severity
C
Bacterial Ratio
***p=2.278e-05
Species Richness
***p=0.0003
Shannon
p=0.1164
non-Critical (n=42)
Critical (n=18)
E
Viral Ratio
***p=2.09e-05
Species Richness
p=0.1120
Shannon
*p=0.0107
F
SARS-Cov-2 Ratio
**p=0.0078
Coronaviridae
**p=0.0074
Herpesviridae
***p=0.0007
Papillomaviridae
*p=0.0180
Poxviridae
**p=0.0015
G
S.aureus
Rate of coinfection
4.34% (1/23)
7.54% (4/53)
0.00% (0/16)
31.6% (5/19)
C. albicans
0.00% (0/23)
1.89% (1/53)
18.8% (3/16)
26.3% (5/19)
log(1+abundance)
Mild
Moderate
Severe
Critical
Sample type
Pharyngeal
Sputum
Relative abundance
High
Low
≥ 1%
< 1%

Figure 3

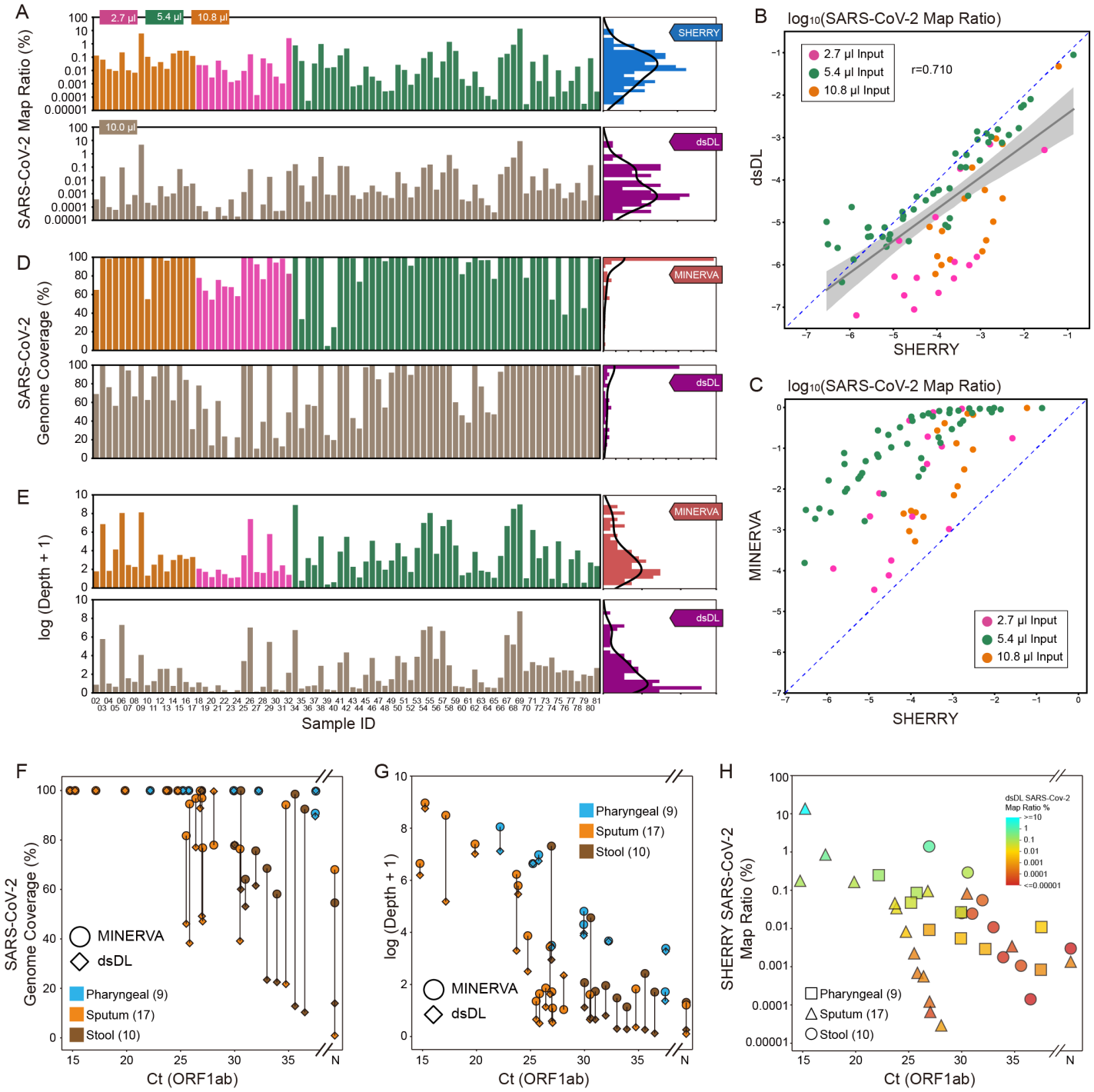
A
2.7 µl
5.4 µl
10.8 µl
10.0 µl
SHERRY
dsDL
SARS-CoV-2 Map Ratio (%)
B
log10(SARS-CoV-2 Map Ratio)
2.7 µl Input
5.4 µl Input
10.8 µl Input
r=0.710
dsDL
SHERRY
C
log10(SARS-CoV-2 Map Ratio)
MINERVA
SHERRY
D
MINERVA
dsDL
SARS-CoV-2 Genome Coverage (%)
E
MINERVA
dsDL
log (Depth + 1)
Sample ID
F
SARS-CoV-2 Genome Coverage (%)
MINERVA
dsDL
Pharyngeal (9)
Sputum (17)
Stool (10)
Ct (ORF1ab)
G
log (Depth + 1)
Pharyngeal (9)
Sputum (17)
Stool (10)
MINERVA
dsDL
Ct (ORF1ab)
H
SHERRY SARS-CoV-2 Map Ratio (%)
dsDL SARS-Cov-2 Map Ratio %
Pharyngeal (9)
Sputum (17)
Stool (10)
Ct (ORF1ab)

Figure 4

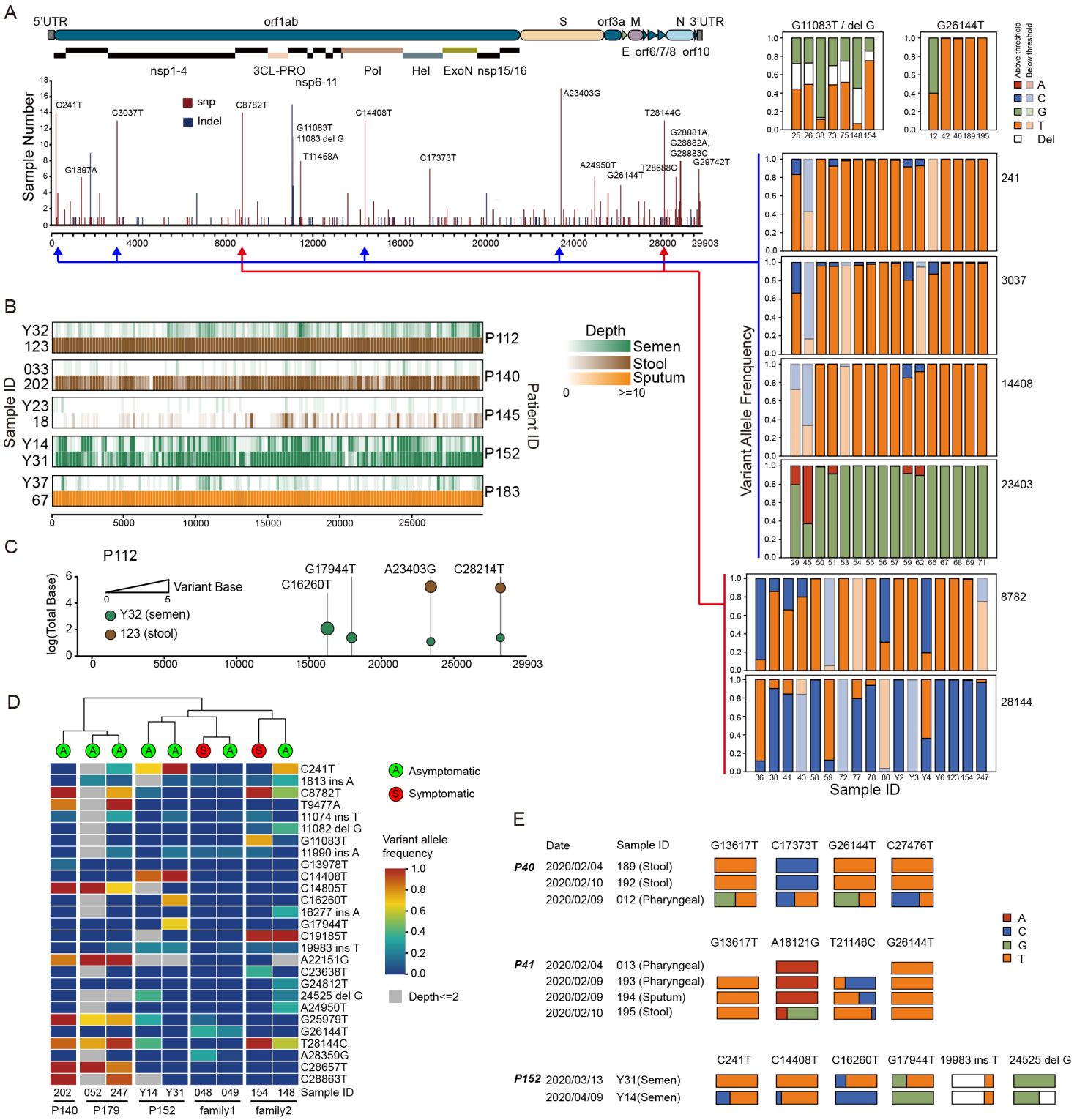
A
5'UTR
orf1ab
S
orf3a
M
N
3'UTR
E
orf6/7/8
orf10
nsp1-4
3CL-PRO
nsp6-11
Pol
Hel
ExoN
nsp15/16
Sample Number
snp
Indel
C241T
C3037T
C8782T
G11083T
11083 del G
C14408T
A23403G
T28144C
G28881A,
G28882A,
G28883C
G29742T
G1397A
T11458A
C17373T
A24950T
G26144T
T28688C
G11083T / del G
G26144T
Above threshold
Below threshold
A
C
G
T
Del
Variant Allele Frenquency
241
3037
14408
23403
8782
28144
Sample ID
B
Y32
123
P112
033
202
P140
Y23
18
P145
Y14
Y31
P152
Y37
67
P183
Sample ID
Patient ID
Depth
Semen
Stool
Sputum
0
>=10
C
P112
log(Total Base)
Variant Base
Y32 (semen)
123 (stool)
G17944T
C16260T
A23403G
C28214T
D
Asymptomatic
Symptomatic
Variant allele frequency
Depth<=2
C241T
1813 ins A
C8782T
T9477A
11074 ins T
11082 del G
G11083T
11990 ins A
G13978T
C14408T
C14805T
C16260T
16277 ins A
G17944T
C19185T
19983 ins T
A22151G
C23638T
G24812T
24525 del G
A24950T
G25979T
G26144T
T28144C
A28359G
C28657T
C28863T
Sample ID
P140
P179
P152
family1
family2
E
Date
Sample ID
G13617T
C17373T
G26144T
C27476T
P40
2020/02/04
189 (Stool)
2020/02/10
192 (Stool)
2020/02/09
012 (Pharyngeal)
A18121G
T21146C
P41
013 (Pharyngeal)
193 (Pharyngeal)
194 (Sputum)
195 (Stool)
C241T
C14408T
C16260T
G17944T
19983 ins T
24525 del G
P152
Y31(Semen)
Y14(Semen)